International Journal of Multiphase Flow 165 (2023) 104485

Contents lists available at ScienceDirect

International Journal of Multiphase Flow

journal homepage: www.elsevier.com/locate/ijmulflow

Comprehensive quasi-steady force correlations for compressible flow through random particle suspensions

Andreas Nygård Osnes [a], Magnus Vartdal [a,*], Mehdi Khalloufi [b,c], Jesse Capecelatro [c], S. Balachandar [d]

[a] Norwegian Defence Research Establishment, PO Box 25, Kjeller, 2007, Norway
[b] Engineering and Process Science, Core R&D, The Dow Chemical Company, Lake Jackson, 77566, TX, USA
[c] Department of Mechanical Engineering, University of Michigan, Ann Arbor, 48109, MI, USA
[d] Department of Mechanical & Aerospace Engineering, University of Florida, Gainesville, 32611, FL, USA

ARTICLE INFO

Keywords:
Drag law
Particle suspensions
Compressible flow
Particle-resolved simulation

ABSTRACT

Models for quasi-steady drag, quasi-steady drag variation, and transverse forces for compressible flows through random, fixed, particle suspensions are presented. Correlations are formulated using drag force measurements obtained from particle-resolved simulation data spanning subsonic to supersonic flow conditions. The newly proposed drag models are extensions of existing models for incompressible dense gas-solid flows to finite Mach numbers, while the transverse particle force model is new and incorporates the covariation between streamwise and transverse forces.

1. Introduction

The effect of fluid compressibility on flows through particle beds is not well established. Many key features of gas-solid flows at moderate to high volume fractions have yet to be determined, such as the effect of finite Mach number on interphase momentum and energy transfer, microscale flow structures, mixing characteristics, chemical reaction rates, attenuation of acoustic signals, etc. Models that capture these effects, and can be applied in macroscale simulations, are crucial for development of technological applications of multiphase flows, as well as for understanding the vast number of natural phenomena in which multiphase flows play an important role. Examples of technological applications and natural phenomena where compressible multiphase flows are important include spacecraft landing (Capecelatro, 2022), pneumatic conveying (Mačak et al., 2021), fuel injection systems (Samareh and Dolatabadi, 2008), and pyroclastic currents (Valentine and Sweeney, 2018).

This work is concerned with the quasi-steady force on a homogeneously distributed particle bed subjected to a spatially uniform ambient flow. The goal is to develop comprehensive particle force models that capture the effects of volume fraction, Reynolds number, and Mach number simultaneously. Models for the mean quasi-steady drag force, the variance of drag force, and the variance of transverse force are sought. To this end, we perform particle-resolved simulations of statistically steady flows through random, fixed, particle beds. This approach is a well-established tool to study gas-solid flows, and has been widely applied in the incompressible regime, for example in Tenneti et al. (2011), Akiki et al. (2016), as well as for shock-induced flows (Mehta et al., 2018; Hosseinzadeh-Nik et al., 2018; Osnes et al., 2019). Data from these simulations, as well as simulation data from other published studies, are used as the basis for model development. An important aspect of the present modeling effort is that the newly developed correlations properly reduce to well-established force models in the incompressible limit of zero Mach number and in the isolated particle limit of zero volume fraction.

A drag law for compressible flows through particle beds was developed recently by Khalloufi and Capecelatro (2023), based on particle-resolved simulations at a superficial Reynolds number of 300. The model is based on the isolated particle drag law of Singh et al. (2022), which was augmented by the finite volume fraction correction factor of Sangani et al. (1991). The authors observed compressibility effects at lower bulk Mach numbers when the particle volume fraction was increased, and in order to capture this effect, they introduced an effective Mach number that depends on the particle volume fraction. Since the Reynolds number was kept constant in this study, the Reynolds number dependence of the drag forces could not be evaluated. Here, we supplement those simulations with simulations at a range of Reynolds numbers, and use both these simulation sets as a basis for determining the Mach number dependency of the forces in compressible particle-laden flows.

* Corresponding author.
E-mail address: magnus.vartdal@ffi.no (M. Vartdal).

https://doi.org/10.1016/j.ijmultiphaseflow.2023.104485
Received 8 March 2023; Received in revised form 10 April 2023; Accepted 11 April 2023
Available online 20 April 2023

Table 1
Parameter combinations simulated in this work.

$\alpha_p = 0.05$		$\alpha_p = 0.1$		$\alpha_p = 0.15$		$\alpha_p = 0.2$		$\alpha_p = 0.2$		$\alpha_p = 0.3$	
$\mathrm{Ma_p}$	$\mathrm{Re_p}$	$\mathrm{Ma_p}$	$\mathrm{Re_p}$	$\mathrm{Ma_p}$	$\mathrm{Re_p}$	$\mathrm{Ma_p}$	$\mathrm{Re_p}$	$\mathrm{Ma_p}$	$\mathrm{Re_p}$	$\mathrm{Ma_p}$	$\mathrm{Re_p}$
0.1	93	0.1	92	0.1	93	0.1	97	0.47	84	0.13	120
0.19	92	0.19	90	0.19	91	0.19	36	0.54	79	0.26	116
0.28	99	0.28	88	0.2	275	0.2	95	0.55	139	0.37	110
0.28	90	0.28	97	0.28	89	0.21	287	0.55	178	0.47	104
0.36	96	0.36	86	0.28	98	0.3	92	0.61	75	0.64	91
0.36	88	0.36	94	0.35	33	0.3	102	0.67	71	0.8	83
		0.64	73	0.37	86	0.36	34	0.68	124		
				0.37	95	0.39	89	0.69	158		
				0.38	258	0.39	98	0.74	68		
				0.65	71	0.39	155	0.81	65		
				0.83	62	0.4	221	0.87	62		
						0.4	266				

2. Problem setup

The governing equations are given by the compressible Navier–Stokes equations. The equation of state of the fluid is taken to be a perfect gas, with an adiabatic index of 1.4. The viscosity is assumed to obey a power law with an exponent of 0.75, and a constant Prandtl number of 0.7 is prescribed. The compressible flow solver CharLES (Brès G.A. Ham et al., 2017) was used to conduct the numerical simulations. The code has been used to study shock-particle cloud interaction (Osnes et al., 2019), and drag forces on isolated particles (Osnes and Vartdal, 2022).

The computational domain is a triply periodic box filled with a random distribution of rigid particles, occupying a mean volume fraction α_p. The particle locations remain fixed throughout the simulation. The dimensions of the boxes are $30D_\mathrm{p} \times 10D_\mathrm{p} \times 10D_\mathrm{p}$ for $\alpha_\mathrm{p} \leq 0.2$, and $15D_\mathrm{p} \times 10D_\mathrm{p} \times 10D_\mathrm{p}$ for $\alpha_\mathrm{p} = 0.3$, where D_p is the diameter of a particle. A minimum distance of $0.02D_\mathrm{p}$ was imposed in order to preserve the control volume quality when two particles are close to each other. The domain is discretized using an unstructured Voronoi-grid with a length scale of $0.02D_\mathrm{p}$ near each particle. Further details regarding grid convergence can be found in Osnes et al. (2019), Osnes and Vartdal (2022).

The boundary conditions on the particle surfaces are isothermal, no-slip, and no-penetration conditions. The fluid flow is driven by a volumetric force in the x-direction, which is constant in time and space. The resulting steady periodic flows are the results of a balance between the volume force and the momentum loss due to particle drag, and a balance between the work done by the body force and the energy loss due to heat conduction across the particle surfaces. The prescribed particle temperature is used as the reference value for the viscosity power law.

The mean flow through the system can be described in terms of the particle volume fraction, Reynolds number, and Mach number

$$\alpha_p = \frac{N_p \pi D_p^3}{6V}, \quad \mathrm{Re_p} = \frac{\langle\rho\rangle \tilde{u} D_\mathrm{p}}{\langle\mu\rangle}, \quad \mathrm{Ma_p} = \frac{\tilde{u}}{\langle c\rangle}, \tag{1}$$

where V is the domain volume, c is the speed of sound, u the mean streamwise velocity, and ρ and μ are the fluid density and dynamic viscosity, respectively. In Eq. (1), $\langle\cdot\rangle$ denotes the average of a quantity over the volume occupied by the fluid phase, and $\tilde{\cdot}$ denotes the corresponding Favre-average. Since both the particle drag and the heat exchange are unknown functions of $\mathrm{Re_p}$, $\mathrm{Ma_p}$, and α_p, the steady state flow conditions produced by a given flow forcing are not known *a priori*. The parameter combinations simulated in this work can be found in Table 1. It should be noted that the simulations in the present work are limited to subsonic mean flow Mach numbers. However, the maximum local Mach numbers typically exceeds the bulk values by a factor of more than two, and significant regions of supersonic flow exist in many of the simulations. The developed correlations also have support in the supersonic bulk Mach number regime from the results in Khalloufi and Capecelatro (2023).

The force on each particle, F_i, includes both the quasi-steady drag force and the undisturbed fluid force, i.e.

$$F_i = F_{\mathrm{qs},i} + F_{\mathrm{un},i}\,. \tag{2}$$

The undisturbed flow force is Annamalai and Balachandar (2017)

$$F_{\mathrm{un,i}} = \frac{\pi D_\mathrm{p}^3}{6}\left[\overline{-\partial_i p^{un} + \partial_j \sigma_{ij}^{un}}^{V_\mathrm{p}}\right], \tag{3}$$

where $\overline{\cdot}^{V_\mathrm{p}}$ denotes the average over the particle volume, and $\cdot^{\mathrm{un}}$ denotes the undisturbed flow of a particle that would exist in the absence of that particle, but in the presence of all other particles. However, in the remainder of this work, we consider the undisturbed fluid flow to be averaged over all the particles and thus is identical for all particles.

The average quasi-steady streamwise, C_D, and transverse, C_T, force coefficients, are

$$C_\mathrm{D} = \frac{8\overline{F}_{\mathrm{qs},1}}{\langle\rho\rangle\tilde{u}^2\pi D_\mathrm{p}^2}, \quad C_\mathrm{T} = \frac{8\sqrt{\overline{F_2^2} + \overline{F_3^2}}}{\langle\rho\rangle\tilde{u}^2\pi D_\mathrm{p}^2}. \tag{4}$$

where for convenience the overline has been omitted from the force coefficients. The average force on each particle deviates from the values of C_D and C_T, and the deviation will be denoted C_D' and C_T'. It should be noted that the definition of C_D differs from that used in Khalloufi and Capecelatro (2023) by a factor $(1-\alpha_\mathrm{p})$.

2.1. Other datasets

In addition to the simulations conducted here, three additional datasets are used for the model development in the following sections. These are the compressible simulations of Khalloufi and Capecelatro (2023), henceforth referred to as KC, and the incompressible simulations of Allahyari et al. (2020) and Seyed-Ahmadi and Wachs (2022). Each of these describe flow through static distributions of monodisperse particles in periodic domains.

The KC simulations span $\alpha_\mathrm{p} \in [0.02, 0.4]$, $\mathrm{Ma_p} \in [0.1, 1.2]$ while keeping the superficial Reynolds number $\mathrm{Re_m} = \mathrm{Re_p}(1-\alpha_\mathrm{p})$ at 300. Unlike the present simulations, adiabatic boundary conditions are enforced at the surface of each particle. Both Allahyari et al. (2020) and Seyed-Ahmadi and Wachs (2022) cover volume fractions in the range $\alpha_\mathrm{p} \in [0.1, 0.4]$. Their respective Reynolds number ranges are $\mathrm{Re_p} \in [7, 121]$ and $\mathrm{Re_p} \in [0.25, 246]$.

3. Streamwise force coefficient model

We use all the results from the current simulations, along with those from the aforementioned datasets, to develop a comprehensive correlation for C_D that captures the effects of $\mathrm{Re_p}$, $\mathrm{Ma_p}$ and α_p simultaneously. We require the model to satisfy the following limiting behaviors. (1) The drag law should reproduce incompressible results in the limit of zero Mach number. (2) It should reproduce isolated particle results

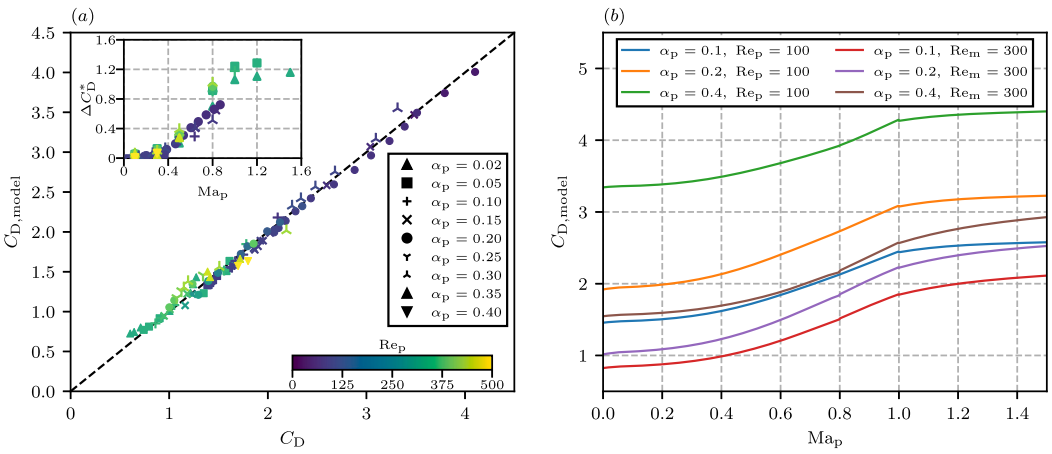

Fig. 1. (a) Streamwise force coefficient model, Eq. (5), as a function of the force coefficient obtained from simulations. The inset axis shows the relative drag coefficient increment, ΔC_D^*, from extrapolated values at $Ma_p = 0$, for each α_p. (b) Model predictions for various combinations of Re_p and α_p.

in the limit of zero volume fraction. Based on these requirements, we propose the following model:

$$C_D\left(\alpha_p, Re_p, Ma_p\right) = \frac{C_{D,Loth}(Re_p, Ma_p)}{\left(1-\alpha_p\right)} + b_3(\alpha_p, Ma_p) + \frac{24\left(1-\alpha_p\right)}{Re_p}\left[b_1\left(\alpha_p\right) + b_2\left(\alpha_p, Re_p\right)\right], \tag{5}$$

where $b_1\left(\alpha_p\right)$ and $b_2\left(\alpha_p, Re_p\right)$ are the volume fraction correction terms identified by Tenneti et al. (2011) as

$$b_1\left(\alpha_p\right) = 5.81\frac{\alpha_p}{\left(1-\alpha_p\right)^2} + 0.48\frac{\alpha_p^{1/3}}{\left(1-\alpha_p\right)^3}, \tag{6}$$

and

$$b_2\left(\alpha_p, Re_p\right) = \left(1-\alpha_p\right)^2\alpha_p^3 Re_p\left[0.95 + 0.61\frac{\alpha_p^3}{\left(1-\alpha_p\right)^2}\right]. \tag{7}$$

To account for finite Mach number effects, we introduce a third correction, given by

$$b_3\left(\alpha_p, Ma_p\right) = \min\left(\sqrt{20Ma_p}, 1\right)\left(5.65\alpha_p - 22\alpha_p^2 + 23.4\alpha_p^3\right) \cdot\left\{1 + \tanh\left[\frac{Ma_p - (0.65 - 0.24\alpha_p)}{0.35}\right]\right\}. \tag{8}$$

The hyperbolic tangent form of the Mach number dependence of b_3 is inspired by the correction for an isolated particle in Loth et al. (2021).

The drag correlation is similar in form to that of Tenneti et al. (2011), in the form reported by Tang et al. (2015). The isolated drag expression, which in Tenneti's correlation is that of Naumann and Schiller (1935), has been replaced by that of Loth et al. (2021).

By replacing the Schiller–Naumann correlation with that by Loth et al. (2021), the correlation is applicable to a broad range of flow conditions at zero volume fraction. Loth's drag correlation is based on a wide range of experimental data, as well as particle-resolved direct numerical simulation (DNS) data. The law covers both incompressible and compressible flows. For finite Mach numbers, it has support for subsonic, transonic, supersonic, hypersonic and rarefied regimes. In the incompressible limit, it tends to the Clift & Gauvin correlation (Clift and Gauvin, 1971), which is applicable for subcritical Re_p.

The present model is compared to the compressible particle-resolved flow simulations in Fig. 1. The model fits the data with a mean square relative error of 4.3%. When $\alpha_p \to 0$, the model tends to the isolated particle drag correlation of Loth et al. (2021). When $Ma_p \to 0$, it tends approximately to the incompressible, finite α_p, drag correlation of Tenneti et al. (2011). It should be noted that because the Loth drag law tends to the Clift & Gauvin correlation, rather than the Schiller–Naumann correlation when $Ma_p \to 0$, the proposed model differs slightly from the model of Tenneti et al. (2011) when $Ma_p \to 0$, $\alpha_p \to 0$. Finally, when $\alpha_p \to 0$, $Ma_p \to 0$, and $Re_p \to 0$, Eq. (5) approaches Stokes drag.

Away from these limits, specifying the models range of validity is non-trivial. The full range of resolved simulation data used to fit the model coefficients are $\alpha_p \in [0, 0.4]$, $Ma_p \in [0, 1.2]$ and $Re_p \in [0.25, 300]$. No tests have been performed beyond these limits.

4. Streamwise force fluctuations

The standard deviation in drag force, σ_F, can be employed in coarse-grained Eulerian–Lagrangian and Eulerian–Eulerian simulations to achieve improved accuracy compared to simulations that employ a model for the mean force only. Lattanzi et al. (2022b) presented a force Langevin model that treats neighbor-induced drag fluctuations as a stochastic force within an Eulerian–Lagrangian framework. In this approach, the drag force is treated as an Ornstein–Uhlenbeck process that requires σ_{CD} as an input. A correlation was developed using data from particle-resolved DNS of fixed particle assemblies valid from $0.1 \leq \alpha_p \leq 0.4$ and $10 \leq Re_p \leq 100$ at $Ma_p = 0$. It was shown that incorporating the unresolved drag force statistics leads to the correct evolution and sustainment of particle velocity variance when compared to particle-resolved simulations of freely evolving homogeneous suspensions. The standard deviation in drag force also plays a role in sources and sinks of fluid-mediated granular temperature in Eulerian–Eulerian two-fluid models (Lattanzi et al., 2022a).

The streamwise force fluctuations were found to be well described by a Gaussian distribution. This property was observed in several incompressible studies, for example Akiki et al. (2016), Lattanzi et al. (2020). The current simulations confirm that this is the case also for compressible flows.

The correlation for σ_F by Lattanzi et al. (2022b) takes the form of the Schiller–Naumann drag force (Naumann and Schiller, 1935), multiplied by a third order polynomial in terms of the volume fraction. The polynomial has an intercept of zero, ensuring that the standard deviation is zero in the limit of zero volume fraction. Here, we extend this correlation to the compressible regime, according to

$$\sigma_F = f_\phi^{\sigma_F}(\alpha_p)F_{single} + b^{\sigma_F}(\alpha_p, Ma_p), \tag{9}$$

where

$$f_\phi^{\sigma_F}(\alpha_p) = 6.52\alpha_p - 22.56\alpha_p^2 + 49.9\alpha_p^3 \tag{10}$$

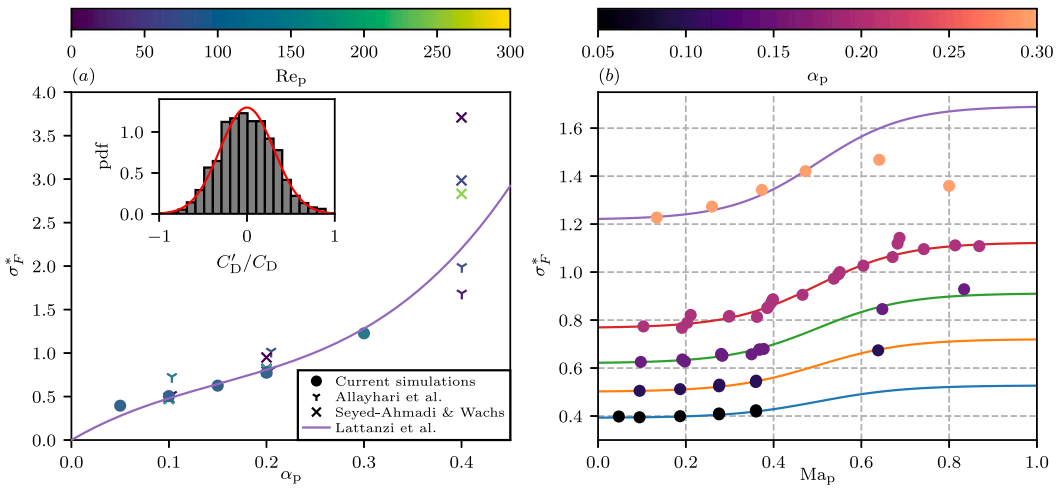

Fig. 2. (a): $\sigma_F^* = \sigma_F/F_{\text{single}}$ as a function of α_p for the incompressible simulations and the compressible simulations with $\text{Ma}_p \approx 0.1$ and the standard deviation model of Lattanzi et al. (2022b). The inset axis in (a) shows the streamwise force fluctuation distribution for $\alpha_p = 0.2$, $\text{Re}_p = 88$ and $\text{Ma}_p = 0.39$, and a Gaussian distribution with mean zero and standard deviation 0.307 (red line). (b): The compressible simulation results (symbols) along with the Mach number correction, Eq. (12) (lines), when matched to the value of σ_F at $\text{Ma}_p = 0.1$. (For interpretation of the references to color in this figure legend, the reader is referred to the web version of this article.)

is the volume fraction polynomial proposed by Lattanzi et al. (2022b),

$$F_{\text{single}} = 3\pi\langle\mu\rangle D_p \left\{1 + 0.15\left[\text{Re}_p(1-\alpha_p)\right]^{0.687}\right\}(1-\alpha_p)\,|\tilde{u}|, \tag{11}$$

and

$$b^{\sigma_F}(\alpha_p, \text{Ma}_p) = \min\left(\sqrt{20\text{Ma}_p}, 1\right) 0.55\alpha_p^{0.7}\left\{1 + \tanh\left[(\text{Ma}_p - 0.5)/0.2\right]\right\}. \tag{12}$$

It should be noted that the Mach number correction to the standard deviation of the streamwise force takes a form closely resembling the Mach number correction in the mean streamwise drag model, Eq. (8), that is an additive correction that increases smoothly as a function of Ma_p before leveling off at supersonic speeds.

Eq. (9) is plotted along with the $\text{Ma}_p \approx 0.1$ simulation data in Fig. 2. The model agrees excellently with the simulation data in the region the volume fraction polynomial was developed for, that is $\alpha_p \geq 0.1$. At $\alpha_p = 0.05$, we observe slightly higher standard deviations than predicted by the model. For the incompressible simulations, there is a spread in the standard deviations and Reynolds number is observed to have a non-negligible effect. However, the Re_p trend is not consistent between the datasets, and we have therefore not attempted to add any Re_p correction to Eq. (9). Fig. 2 also shows the Mach number correction, Eq. (12), plotted alongside the current simulation results as a function of Ma_p. Eq. (12) captures the Ma_p trend quite well except for $\alpha_p = 0.3$ at $\text{Ma}_p > 0.5$. At $\alpha_p = 0.3$, the difference in Re_p between the low and high Mach number simulations is the reason the higher Mach number results appear to deviate from the trend.

5. Transverse force coefficient

In this section we consider the force on the particle normal to the flow direction (the lift force). This transverse force is correlated to the drag force in the streamwise direction, and in general high streamwise forces are often accompanied by large transverse forces.

Akiki and Balachandar (2020) found that the two flow-normal components of the forces were normally distributed at low Reynolds numbers and proposed a stochastic model for the lift force. Normally distributed transverse forces were found for the current simulations as well. Since the current systems are axisymmetric, the two transverse force components are uncorrelated, and the magnitude of the transverse force can be equivalently described by a Rayleigh distribution.

The covariance of C_D', and C_T can be used to compute a value of C_T for each C_D'. To this end, we compute the conditional pdfs of C_T for five categories of C_D'. The fluctuating drag coefficient is categorized as large negative, negative, neutral, positive or large positive, corresponding to the intervals $\left(\infty, -\sigma_{C_D}\right]$, $\left(-\sigma_{C_D}, -\sigma_{C_D}/3\right]$, $\left(-\sigma_{C_D}/3, \sigma_{C_D}/3\right]$ $\left(\sigma_{C_D}/3, \sigma_{C_D}\right]$, and $\left(\sigma_{C_D}, \infty\right)$. The conditional pdfs show functional dependencies on α_p, Re_p and Ma_p. A model for the conditional pdfs is therefore

$$C_T(\alpha_p, \text{Re}_p, \text{Ma}_p, C_D') = C_D\left(\alpha_p, \text{Re}_p, \text{Ma}_p\right) c_T(\alpha_p, \text{Re}_p, \text{Ma}_p, C_D'), \tag{13}$$

where c_T follows the Rayleigh distribution, given by

$$\Pr(c_T = \xi) = \frac{\xi}{\sigma_{C_T}^2}\exp\left(-\frac{\xi^2}{2\sigma_{C_T}^2}\right), \tag{14}$$

where

$$\sigma_{C_T}(\alpha_p, \text{Re}_p, \text{Ma}_p, C_D') = \frac{A_1(C_D')\alpha_p}{A_2(C_D') + \alpha_p}\left[A_3(C_D') + A_4(C_D')\log\left(1 + \text{Re}_p\right) + A_5(C_D')\text{Ma}_p\right]. \tag{15}$$

The values of A_1 to A_5 are reported in Table 2. While the model is defined as a piecewise constant function of C_D', a continuous function for C_T can be obtained through an interpolation procedure based on Table 2.

When the streamwise force is low ($C_D' \leq -\sigma_{C_D}/3$), σ_{C_T} has no Reynolds number dependence. This can be understood because the lowest streamwise forces occur for particles in regions where the flow speed is low, for example immediately behind another particle. These regions exist in the flow for all Re_p considered here, and thus the streamwise force distribution for particles located in these regions is independent of Re_p. For higher C_D', there is a Reynolds number dependence, where high Re_p corresponds to high σ_{C_T}. On the other hand, σ_{C_T} has a stronger dependence on Ma_p when the streamwise force is low.

The distributions of the transverse force predicted by this model are shown for four flow conditions in Fig. 3. Generally, the distribution of c_T is wider when C_D' is large. The mode of the distribution is typically about 20% of the streamwise force, unless the Reynolds number is low or the volume fraction is below 5%. In case of a planar curtain of particles, the transverse motion of the particles resulting from the transverse force averages out without affecting the uniform particle distribution along the transverse direction within the curtain. In contrast, in case of a finite lateral patch of particles, as those considered by Boiko et al.

Table 2
Coefficients for the transverse force model.

	$10 \cdot A_1$	$10 \cdot A_2$	$10 \cdot A_3$	$10 \cdot A_4$	$10 \cdot A_5$
$C'_{\mathrm{D}} \leq -\sigma_{C_{\mathrm{D}}}$	1.29	0.55	13.3	0	3.42
$-\sigma_{C_{\mathrm{D}}} < C'_{\mathrm{D}} \leq -\sigma_{C_{\mathrm{D}}}/3$	1.24	0.36	14.3	0	4.83
$-\sigma_{C_{\mathrm{D}}}/3 < C'_{\mathrm{D}} \leq \sigma_{C_{\mathrm{D}}}/3$	0.96	0.19	17.4	0.53	4.70
$\sigma_{C_{\mathrm{D}}}/3 < C'_{\mathrm{D}} \leq \sigma_{C_{\mathrm{D}}}$	1.68	0.14	10.1	0.44	3.69
$\sigma_{C_{\mathrm{D}}} \leq C'_{\mathrm{D}}$	0.49	0.06	33.2	4.20	4.29

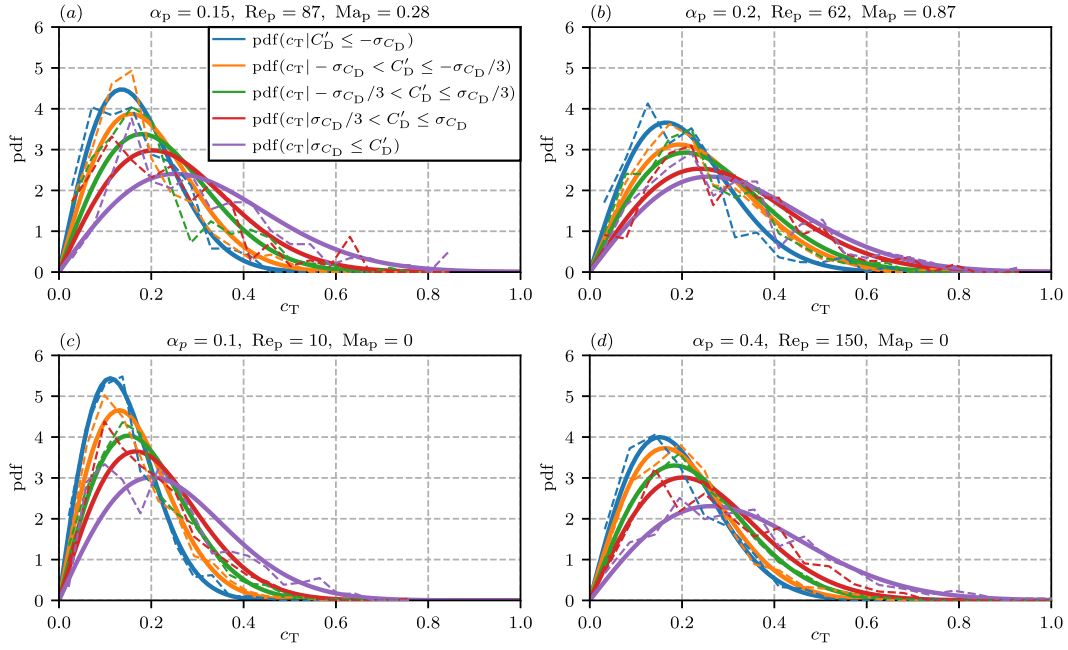

Fig. 3. Distribution of the normalized transverse force coefficients for four flow conditions. Solid lines: Eqs. (14) and (15); dashed lines: Simulation distributions.

(1997), the transverse force will contribute to transverse spreading of the patch, as observed in their experiments.

6. Concluding remarks

In this study, we propose models for the quasi-steady forces acting on particles in compressible, homogeneous flows through random, fixed, particle suspensions. The models are based on particle-resolved simulation data from both compressible (Khalloufi and Capecelatro, 2023) and incompressible (Allahyari et al., 2020; Seyed-Ahmadi and Wachs, 2022) simulations. In the current work, simulations of compressible dense gas-solid flows, supplementing the simulation data of Khalloufi and Capecelatro (2023), were conducted in order to explore the Ma_{p} dependence of quasi-steady streamwise and transverse forces.

We developed a model for the mean streamwise, quasi-steady drag, which extends and combines the drag models of Tenneti et al. (2011) and Loth et al. (2021) to finite Ma_{p} and finite α_{p}. The Mach number correction at finite α_{p} takes the form of a smooth increase up to supersonic flows, after which it remains constant. We find that the drag increase occurs earlier for higher α_{p}, which has previously been observed by Khalloufi and Capecelatro (2023).

We also developed a model for the standard deviation of the streamwise drag force. The model extends that proposed by Lattanzi et al. (2020) to the finite Ma_{p} regime. In Lattanzi's model the α_{p} dependence is captured by a third degree polynomial. We augmented this model with an additive term that captures the change as Ma_{p} increases. We found that the streamwise drag variation increases smoothly as a function of Ma_{p}, and reaches a plateau at high transonic flow.

Finally, a model for the transverse force variation in the form of a stochastic model that captures the covariation of streamwise and transverse forces was also developed. The transverse forces were found to be normally distributed, and that high streamwise drag forces were correlated to high transverse forces.

By conducting new particle-resolved simulations and gathering results from existing simulations of uniform flow over a homogeneous random distribution of stationary particles at varying Reynolds number, Mach number, and volume fraction comprehensive models of mean and fluctuating components of quasi-steady streamwise and transverse forces have been developed.

Although the models have been developed for static particulate systems we envision these correlations to represent an important step towards achieving system-scale numerical simulations of compressible gas-solid flows of finite volume fraction.

CRediT authorship contribution statement

Andreas Nygård Osnes: Conceptualization, Methodology, Formal analysis, Investigation, Data curation, Writing of first draft, Revision. **Magnus Vartdal:** Conceptualization, Methodology, Investigation, Writing of first draft, Revision. **Mehdi Khalloufi:** Methodology, Data curation. **Jesse Capecelatro:** Formal analysis, Writing of first draft, Revision. **S. Balachandar:** Conceptualization, Investigation, Writing of first draft.

Declaration of competing interest

The authors declare that they have no known competing financial interests or personal relationships that could have appeared to influence the work reported in this paper.

Data availability

Data will be made available on request.

Acknowledgments

JC and MK acknowledge support by NASA, United States grant no. 80NSSC20K0295. SB acknowledges support by the U.S. Department of Energy, Stewardship Science Academic Programs, under Contract No. DE-FOA-0002457

Appendix A. Supplementary data

Supplementary material related to this article can be found online at https://doi.org/10.1016/j.ijmultiphaseflow.2023.104485.

References

Akiki, G., Balachandar, S., 2020. Shear-induced lift force on spheres in a viscous linear shear flow at finite volume fractions. Phys. Fluids 32, 113306.
Akiki, G., Jackson, T.L., Balachandar, S., 2016. Force variation within arrays of monodisperse spherical particles. Phys. Rev. Fluids 1, 044202.
Allahyari, M., Moore, W., Siddani, B.S., Balachandar, S., 2020. A deep neural network-based approach for the force predictions of particulate multiphase flows. In: APS Division of Fluid Dynamics Meeting Abstracts. pp. J12–011.
Annamalai, S., Balachandar, S., 2017. Faxén form of time-domain force on a sphere in unsteady spatially varying viscous compressible flows. J. Fluid Mech. 816, 381–411.
Boiko, V., Kiselev, V., Kiselev, S., Papyrin, A., Poplavsky, S., Fomin, V., 1997. Shock wave interaction with a cloud of particles. Shock Waves 7, 275–285.
Brès G.A. Ham, F.E., Nichols, J.W., Lele, S.K., 2017. Unstructured large-eddy simulations of supersonic jets. AIAA J. 116, 4–1184.
Capecelatro, J., 2022. Modeling high-speed gas–particle flows relevant to spacecraft landings. Int. J. Multiph. Flow. 150, 104008.
Clift, R., Gauvin, W., 1971. Motion of entrained particles in gas streams. Can. J. Chem. Eng. 49, 439–448.
Hosseinzadeh-Nik, Z., Subramaniam, S., Regele, J.D., 2018. Investigation and quantification of flow unsteadiness in shock-particle cloud interaction. Int. J. Multiph. Flow. 101, 186–201.
Khalloufi, M., Capecelatro, J., 2023. Drag force of compressible flows past random arrays of spheres. Int. J. Multiphase Flow (Accepted for publication).
Lattanzi, A.M., Tavanashad, V., Subramaniam, S., Capecelatro, J., 2020. Stochastic models for capturing dispersion in particle-laden flows. J. Fluid Mech. 903.
Lattanzi, A.M., Tavanashad, V., Subramaniam, S., Capecelatro, J., 2022a. Fluid-mediated sources of granular temperature at finite Reynolds numbers. J. Fluid Mech. 942.
Lattanzi, A.M., Tavanashad, V., Subramaniam, S., Capecelatro, J., 2022b. Stochastic model for the hydrodynamic force in Euler–Lagrange simulations of particle-Laden flows. Phys. Rev. Fluids 7, 014301.
Loth, E., Tyler Daspit, J., Jeong, M., Nagata, T., Nonomura, T., 2021. Supersonic and hypersonic drag coefficients for a sphere. AIAA J. 59, 3261–3274.
Mačak, J., Goniva, C., Radl, S., 2021. Regimes of subsonic compressible flow in gas-particle systems. Powder Tech. 394, 44–61.
Mehta, Y., Neal, C., Salari, K., Jackson, T.L., Balachandar, S., Thakur, S., 2018. Propagation of a strong shock over a random bed of spherical particles. J. Fluid Mech. 839, 157–197.
Naumann, Z., Schiller, L., 1935. A drag coefficient correlation. Z. Ver. Deutsch. Ing. 77, e323.
Osnes, A.N., Vartdal, M., 2022. Mach and Reynolds number dependency of the unsteady shock-induced drag force on a sphere. Phys. Fluids 34, 043303.
Osnes, A.N., Vartdal, M., Omang, M.G., Reif, B.A.P., 2019. Computational analysis of shock-induced flow through stationary particle clouds. Int. J. Multiph. Flow 114, 268–286.
Samareh, B., Dolatabadi, A., 2008. Dense particulate flow in a cold gas dynamic spray system. J. Fluids Eng. 130, 081702.
Sangani, A.S., Zhang, D., Prosperetti, A., 1991. The added mass, basset, and viscous drag coefficients in nondilute bubbly liquids undergoing small-amplitude oscillatory motion. Phys. Fluids 3, 2955–2970.
Seyed-Ahmadi, A., Wachs, A., 2022. Physics-inspired architecture for neural network modeling of forces and torques in particle-Laden flows. Comput. & Fluids 238, 105379.
Singh, N., Kroells, M., Li, C., Ching, E., Ihme, M., Hogan, C.J., Schwartzentruber, T.E., 2022. General drag coefficient for flow over spherical particles. AIAA J. 60, 587–597.
Tang, Y., Kuipers, F., Peters, H., Kriebitzsch, S., van der Hoef, M., 2015. A new drag correlation from fully resolved simulations of flow past monodisperse static arrays of spheres. AIChE J. 61, 688–698.
Tenneti, S., Garg, R., Subramaniam, S., 2011. Drag law for monodisperse gas–solid systems using particle-resolved direct numerical simulation of flow past fixed assemblies of spheres. Int. J. Multiph. Flow. 37, 1072–1092.
Valentine, G.A., Sweeney, M.R., 2018. Compressible flow phenomena at inception of lateral density currents fed by collapsing gas-particle mixtures. J. Geophys. Res. 123, 1286–1302.